JOURNAL OF GEOPHYSICAL RESEARCH, SPACE PHYSICS VOL. 74, NO. 26, DECEMBER 1, 1969

Whistler-Mode Emissions on the OGO 1 Satellite

N. DUNCKEL AND R. A. HELLIWELL

Radioscience Laboratory
Stanford University, Stanford, California 94305

Magnetospheric observations of whistler-mode emissions were made by the OGO 1 satellite over the frequency range 0.3 to 100 kHz. Taken during the geomagnetically quiet period from September 1964 through May 1965, the data cover geocentric distances from 2 to 24 R_E and geomagnetic latitudes in the range $\pm 50°$. Emissions are found within $L \sim 10$ at all local times except for $L > 5$ in the midnight-to-dawn sector, with intensity peaking at $L \sim 4$ and $L \sim 9$ near 10 hours local mean time. Their spectra resemble those of chorus and mid-latitude hiss observed on the ground. An important new result is the observation that the upper-frequency limit of most of these emissions is proportional to the minimum electron gyrofrequency along the magnetic fieldline passing through the satellite. This is interpreted to mean that the source of these emissions lies close to the equatorial plane. Estimates of the average intensity of these emissions agree with the intensity required to explain the precipitation of electrons through pitch-angle scattering by whistler-mode waves. Emissions observed on the dayside beyond $L = 8$ are burst-like, and their occurrence tends to decrease with increasing radial distance. The location of the maximum intensity in this region agrees with that found for 1-kev electron fluxes, giving strong support to theories of generation based on electron cyclotron resonance. No emissions were observed beyond the estimated position of the shock boundary.

INTRODUCTION

The Stanford University/Stanford Research Institute VLF experiment on the OGO 1 satellite provided the first opportunity for detailed measurements of VLF emission spectra and intensity at high altitudes near the equatorial plane where certain classes of these emissions are believed to be generated. Until recently, low-frequency waves from the magnetosphere have been observed either with ground stations [cf. *Helliwell*, 1965, and references therein] or with low-altitude satellites [*Barrington et al.*, 1963; *Barrington*, 1969; *Gurnett and O'Brien*, 1964, *Jørgensen*, 1968; *Scarf et al.*, 1968; *Taylor and Gurnett*, 1968]. Ground observations are largely limited to signals traveling in ducts (field-aligned enhancements of ionization) since reflection and absorption prevent nonducted signals from penetrating the ionosphere [*Helliwell*, 1965]. Low-altitude satellites provide access to nonducted signals but do not observe downward-propagating emissions that have been reflected or absorbed at higher altitudes.

Here we describe the occurrence, intensity, and spectra of emissions observed by OGO 1 at frequencies below the local electron gyrofrequency. The spectra resemble those observed on the ground and include hiss, random chorus, periodic chorus, and triggered emissions. A new and important spectral feature is a marked upper cutoff that is proportional to the minimum gyrofrequency on the fieldline through the satellite. From this result we conclude that the region of the observed emissions lies close to the equatorial plane.

The present study provides the first direct test of the *Kennel and Petschek* [1966] theory, which states that the maximum flux of trapped particles is limited by pitch-angle diffusion due to interaction with whistler-mode waves. A consequence of the theory is that the emissions must have a certain field strength. Previous measurements, by low-altitude satellites, were made too far from the generation region to be reliable. The average wideband noise intensities near the equator estimated from the data reported are comparable to the fields required by the Kennel-Petschek theory.

Closely related to the present work is a companion study of a VLF emission form called banded chorus, observed on OGO 1 and OGO 3 [*Burtis and Helliwell*, 1969]. In addition to confirming that the frequency of the chorus

TABLE 1. Receiver Characteristics

Parameter	Band 1 Receiver	Band 2 Receiver	Band 3 Receiver	Broadband Receiver
Frequency range	0.2–1.6 kHz	1.6–12 kHz	12–100 kHz	0.3–13 kHz
Background noise intensity	$4 \times 10^{-5}\gamma$ Hz$^{-1/2}$ at 0.8 kHz	$2 \times 10^{-6}\gamma$ Hz$^{-1/2}$ at 6.0 kHz	$4 \times 10^{-7}\gamma$ Hz$^{-1/2}$ at 55 kHz	$2 \times 10^{-4}\gamma$ Hz$^{-1/2}$ (0.3 kHz) to $2 \times 10^{-6}\gamma$ Hz$^{-1/2}$ (12.5 kHz)
Bandwidth −3 db/−60 db	40/450 Hz	160/1300 Hz	600/4500 Hz	
ΔF/Step	5.4 Hz	43 Hz	344 Hz	
Output time constant at 64/8/1 kilobit/sec	14/110/880 msec	4.4/49/340 msec	2/18/150 msec	
Sweep time at 64/8/1 kilobit/sec		2.3/18.4/147 sec		

depends upon the minimum gyrofrequency along the fieldline passing through the satellite, this separate study led to a new result regarding the frequency of generation. It was found that when the deviations of a nonducted ray path from the fieldline were considered, the frequency of generation was close to one-half the gyrofrequency in the equatorial plane.

In addition to the VLF emissions that exhibit a high-frequency cutoff below the local electron gyrofrequency, OGO 1 observes two types of noise extending in frequency to the upper limit of the receiver (100 kHz) [*Dunckel et al.*, 1969]. One is called 'highpass' noise and exhibits a variable low-frequency cutoff above about 20 kHz. The other is called 'broadband' noise and covers the entire frequency range of the receiver. Both types are observed within the magnetosphere in association with polar substorm activity. Virtually never do they occur simultaneously with whistler-mode noise.

Experiment

A single-turn loop antenna (diameter = 2.9 meters) and preamplifier feed four receivers with logarithmic response. (For further details see *Rorden et al.* [1966].) For circularly polarized waves of random orientation the response is within 6 db of the maximum 86% of the time. Thus only rarely should the directional response of the loop antenna markedly affect the intensity measurements.

Three of the receivers are simultaneously stepped in frequency to produce an amplitude spectrum over the effective range 0.3 to 100 kHz in three bands. Each sweep of 256 steps requires 2.3 seconds or longer depending upon the rate of data transmission. Pertinent details appear in Table 1. (The noise bandwidths of receivers of similar design (OGO 4) were found to be ½ the 3-db bandwidth. Intensities based on the 3-db bandwidth should be increased by 3 db to account for the different effective bandwidth.) The dynamic range of each receiver is at least 80 db. An alternative mode of operation permits the three receivers to be stopped at any given step to produce the amplitude at three fixed frequencies versus time. A fourth receiver, called the broadband receiver, produces the amplitude-limited waveform of signals in the range 0.3–13 kHz for detailed spectral analysis on the ground. All receivers are periodically calibrated by a 1-kHz sawtooth wave of known harmonic content inserted periodically at the antenna. Two transmitters in the satellite provide the analog and pulse-code modulation telemetry used by the broadband and sweeping receivers, respectively.

The data from the sweeping receivers have been computer-processed and recorded on 16-

mm film [*Ficklin et al.*, 1967], so that one frame represents a sweep of each of the three sweeping receivers as shown in Figure 1*b*, to be discussed in detail later. The background noise level, determined by the receiver noise plus spacecraft interference at 0.4 kHz, 2.46 kHz, and their harmonics, has been derived from quiet-time data and is shown as a light dashed line.

The waveforms from the broadband receiver have been spectrum-analyzed as shown in Figure 1*a*. The nonlinearity of the receiver causes its output to be dominated by the strongest signal in its passband, as illustrated by the whistler near the right-hand edge of Figure 1*a*. Strong fields below 1 kHz may appear only faintly in the broadband data, as in Figures 1*a* and 2*a*, since the broadband receiver weights the magnetic intensity by a factor approximately proportional to frequency.

The OGO 1 satellite itself is described in the literature [*IG Bulletin*, 1965]. The satellite exhibits an unintended rotation about an axis that lies within about 7° of the axis of the loop antenna. Hence modulation of whistler-mode signals at the period of rotation is not expected, nor has it been observed.

Results

Types of observations. The emissions discussed here are observed below the estimated local electron gyro- and plasma frequencies, and thus are called 'whistler-mode' emissions. *Hiss* appears as a continuous spectrum showing little change over several seconds as shown in Figure 1*a*. *Discrete* emissions appear on a spectrogram as forms isolated in frequency and time as illustrated by the rising elements in Figure 2*a*, or as bursts such as that shown in Figure 2*c*. Often hiss and discrete emissions occur together as in Figure 2*a*. The appearance of these emissions in the output of the sweeping receivers (Figures 2*b*, 2*d*) differs markedly from that of whistlers and manmade signals. In the regions where all three phenomena occur, emissions are either of long duration or have an appreciable bandwidth so that their identification is unambiguous.

Typical emissions. From $L = 2.5$ out to the vicinity of the plasmapause (usually near $L = 4$), a strong band of hiss of relatively constant intensity often appears from the low-frequency limit of observation, 0.3 kHz, to as high as 3 kHz. An example of this hiss extending to relatively high frequencies (~2 kHz) is shown in Figure 1. Part (*a*) shows the spectrum-analyzed output from the broadband receiver, and part (*b*) shows for the same interval the amplitude spectrum from the sweeping receivers in db below one gamma. The position of the satellite appears in terms of R, the geocentric distance in earth radii; MLAT, the dipole magnetic latitude; L in earth radii based on a Jensen-Cain magnetic field model; LMT, the local mean time in hours; SEP, the sun-earth-probe angle in degrees; and f_{H0}, the minimum f_H along the fieldline passing through the satellite, where f_H = electron gyrofrequency in kHz based on a magnetic field model (discussed later) which includes the compression effects of the solar wind. The background level is shown as a light dashed line in the upper two graphs of Figure 1*b*. The locus of the sweeps of the band 1 and band 2 receivers has been drawn on the spectrum of part (*a*). A whistler of low dispersion ($D \approx 13$ sec$^{1/2}$) appears in the spectrum (*a*) near the right-hand edge. The emission spectrum shows no obvious structure, but slowly decreases in intensity from 0.2 kHz to 2 kHz; from 2 kHz to 2.5 kHz the intensity drops rapidly through 30 db to the threshold level.

In the vicinity of the plasmapause, a narrow band of hiss-like emissions often appears at frequencies above 0.4 f_{H0} and persists over $\Delta L = 0.1$ to 0.5. Unpublished data from the OGO 1 ion mass spectrometer [*Taylor et al.*, 1965] has confirmed that these emissions occur near the plasmapause.

From the plasmapause out through the transition region the emissions often become more discrete and their upper-cutoff frequency decreases with increasing L value. Figures 2*a* and 2*b* show the dynamic and amplitude spectra, respectively, of emissions at $L = 9.5$ in which discrete elements near 0.7 kHz are superimposed on hiss below 0.6 kHz. A sharp upper cutoff occurs at 0.7 kHz, or 0.28 f_{H0}. (In the dynamic spectra of Figures 1*a* and 2*a* the apparent low-frequency cutoff is caused by the broadband receiver response, not by a lack of signal.)

Outside the plasmapause the spectra of the emissions vary considerably. In the present study of data recorded before June 1965, it

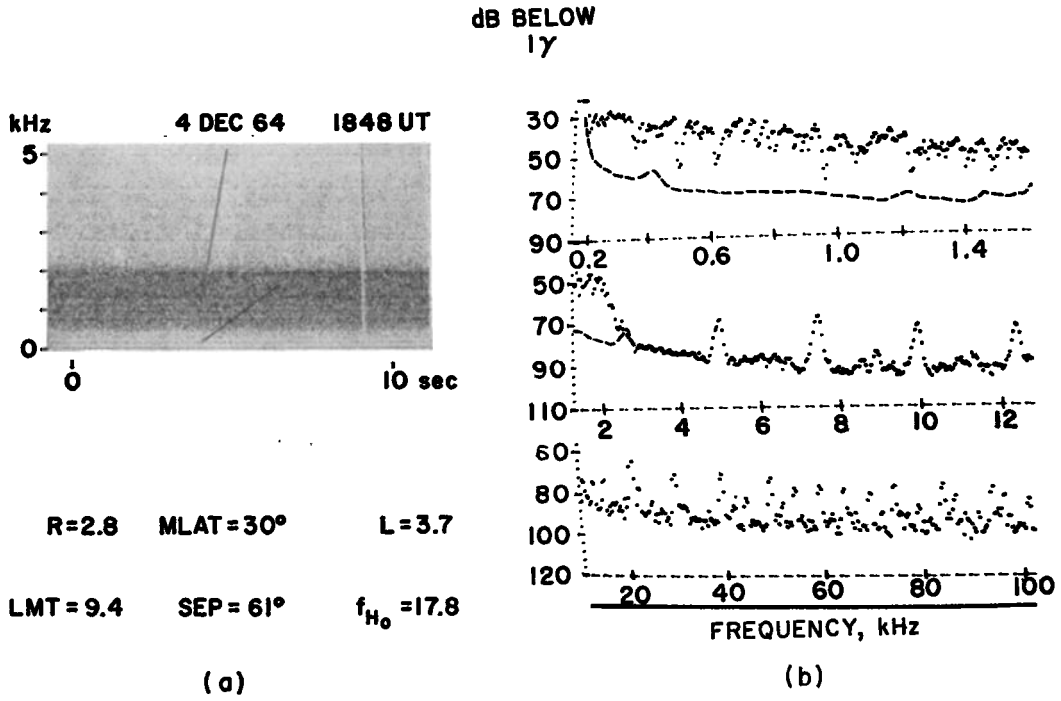

Fig. 1. Example of emissions received by OGO 1 inside plasmapause. (*a*) High-resolution spectrum from broadband receiver. (*b*) Amplitude spectrum from three sweeping receivers; vertical axes are labeled in terms of equivalent intensity of a single frequency signal in db below one gamma (20 db corresponds to a ten-fold change in magnetic intensity); horizontal axes represent frequency in kHz; dashed lines represent background level. Noise band cuts off at 2.3 kHz. The two upward-sloping lines in (*a*) were drawn to represent locus of sweeps corresponding to upper two graphs of (*b*). Faint horizontal lines are interference. Lack of pronounced discrete elements and smoothly decreasing intensity with increasing frequency are characteristic of this region. Note whistler in right-hand part of (*a*).

was found that the spectrum of most emissions extended from below 0.3 kHz to the upper-cutoff frequency. Measurement of a few cases indicates that the wave magnetic field strength tends to vary as the nth power of the frequency, where n varies between -1 and -3. However, *Burtis and Helliwell* [1969] noted that emissions observed by OGO 1 and OGO 3 outside the plasmapause during the latter half of 1966 occurred primarily in a narrow band of frequencies. Hence a secular variation may exist.

In the distant magnetosphere, the emissions become more sporadic. Figures 2*c* and *d* show the spectra and intensity of an event recorded at a dipole L of 13.3. The emissions occur between 450 and 800 Hz, and consist of a short burst and a relatively long (>10 sec) burst. Similar events on the same pass occurred every few minutes.

The intensity and the occurrence of the emissions decrease when the radial distance of the satellite exceeds 10 to 15 R_E; this is the approximate radial distance of the magnetopause on the dayside as indicated by the OGO 1 search-coil magnetometer [*Holzer et al.*, 1966]. At the location of the shock boundary on one pass [*Holzer et al.*, 1966, Figure 1*c*], weak emissions up to several kHz were observed by our experiment. No emissions were observed when the satellite was clearly outside the shock boundary.

Inside the plasmapause the emissions received on passes through the night magnetosphere are

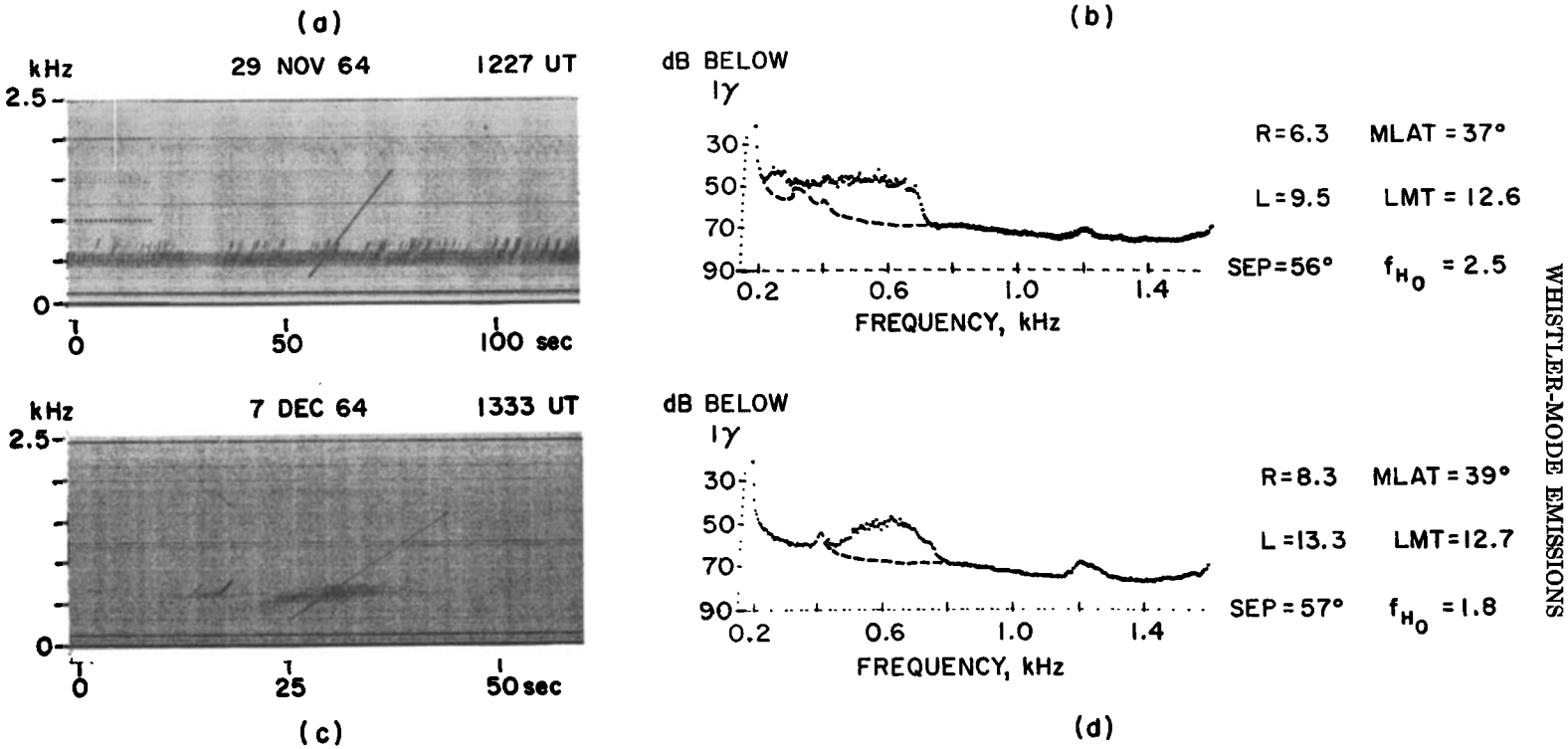

Fig. 2. Examples of emissions received by OGO 1 between the plasmapause and the magnetopause. High-resolution spectra from broadband receiver appear at left and amplitude spectra from band 1 sweeping receiver appear at right in units of db below one gamma as a function of frequency in kHz. Dashed lines represent background level. Dark sloping lines in (*a*) and (*c*) were drawn to represent locus of sweeps shown in (*b*) and (*c*). Dot pattern at multiples of 1 kHz at beginning of (*a*) is made by the inflight calibration signal. Vertical striations in (*a*) and (*c*) are due to telemetry fading as satellite rotates. A Williams-Mead field model was used to determine f_{H0}.

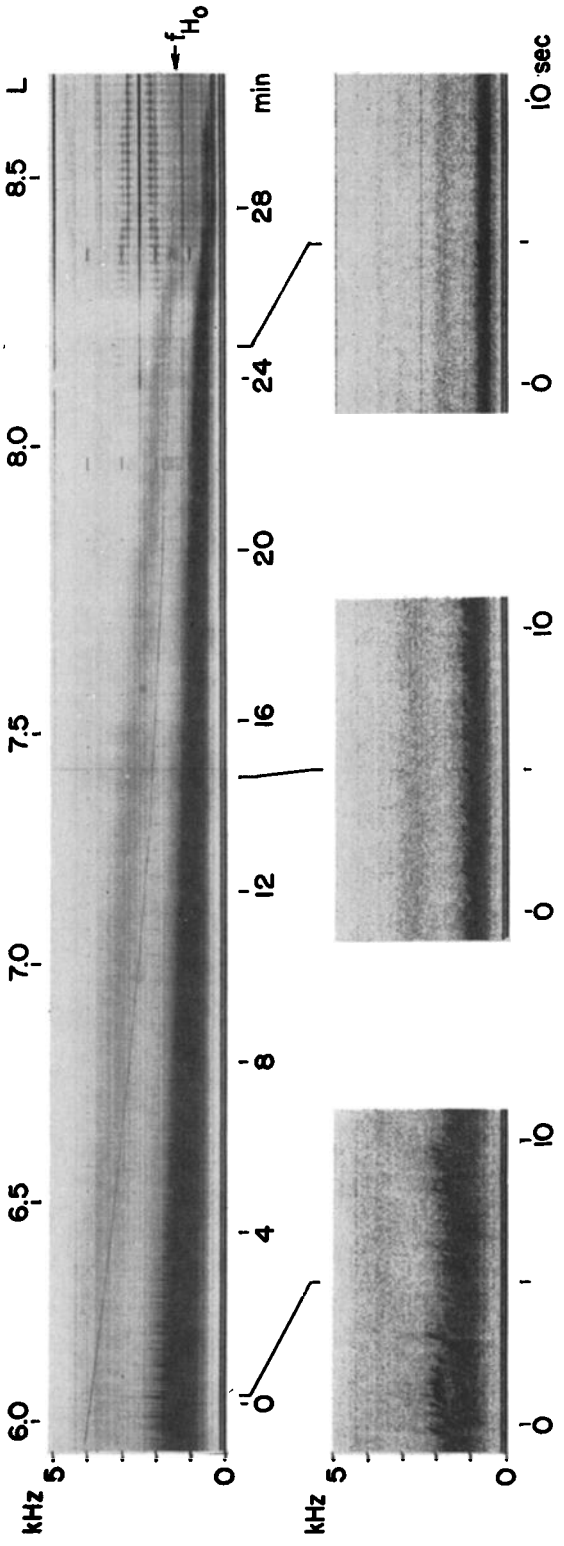

Fig. 3. Broadband receiver spectra showing systematic variation of upper-cutoff frequency with change in L (indicated at top of upper panel). Three samples of the spectra on an expanded time scale are shown in the lower panel and illustrate a typical pattern of rising elements superimposed on a continuum. The value of f_{H0} calculated from the Jensen-Cain model has been drawn on upper panel for comparison. For the period shown the magnetic latitude remained at 41° ± 1° and the local mean time at 15.0 ± 0.8 hours. Calibration signal at multiples of 1 kHz appears clearly near 22 and 27 minutes and faintly before 21 minutes. Horizontal lines are interference. Weak third harmonic of emissions is generated by limiting action in broadband receiver. Note that ratio of upper-cutoff frequency to f_{H0} remains approximately constant.

similar to those on the dayside. Outside the plasmapause, particularly in the post-midnight period, strong emissions of the type seen on the dayside are seldom observed. Highpass and broadband noises are common, and noise resembling auroral hiss observed at ground stations [*Martin et al.*, 1960] is sometimes observed.

Upper-cutoff frequency. A characteristic feature of the whistler-mode emissions observed on the OGO 1 satellite is an upper-cutoff frequency that varies with the position of the satellite and tends to be proportional to f_{H0}. This upper cutoff is quite abrupt, as shown by Figure 1, where the intensity decreases at the rate of about 45 db/octave in the vicinity of the cutoff. Discrete emissions also have a marked upper cutoff as shown in the Figures 2*a–b*, where rising discrete elements display a common upper cutoff somewhat above that of the hiss. The emission of Figure 2*c* shows nearly symmetrical upper and lower cutoffs.

Systematic variation of the upper-cutoff frequency with position of the satellite is illustrated in Figure 3, which shows the dynamic spectrum recorded on an outbound pass from $L = 5.9$ to $L = 8.7$. The lower panel shows three samples of data on an expanded time scale. The emissions consist of discrete risers superimposed on a broadband continuum, the discrete elements becoming less pronounced as the satellite travels outward. In the upper record the value of f_{H0} based on a Jensen-Cain field has been drawn in lightly for comparison. The upper cutoff, defined as the frequency above which no external noise can be detected, lies between about 0.45 and 0.65 f_{H0} during all but the last minute of the record. (Note the following effects produced by the equipment: the band just above f_{H0} representing the third harmonic of the emissions; the vertical striations at the end of the upper panel caused by telemetry fading; and the apparent variation of the lower-cutoff frequency.)

The amplitude spectra in the region of the upper-cutoff frequency are shown in Figure 4 for portions of the same pass as shown in Figure 3. The frequency has been normalized by f_{H0}, and the amplitudes have been normalized to a 1-Hz bandwith. The range of normalized cutoffs was significantly reduced by employing a compressed field model (discussed later) of the earth's magnetic field to determine f_{H0}. In the range $5.5 \leq L \leq 7$ the graphs shown were averaged from three frames of 64 kilobit/sec data to provide a smoother curve. Data from higher L were taken at 8 kilobits/sec and required no further averaging. In the vicinity of the upper-cutoff frequency the emissions have a normalized spectrum that is relatively independent of the location of the satellite. The sample showing the most deviation, that taken at $L = 9.0$, was recorded when the emissions were dying out. Attenuation rates in the region of the upper-cutoff frequency range from 20 to over 70 db per octave.

Magnetic field model. The upper-cutoff frequencies have been compared to local (f_H) and minimum (f_{H0}) electron gyrofrequencies based on a magnetic field model in which the effects of compression by the solar wind and of a tail field are included [*Williams and Mead*, 1965]. Henceforth this model is referred to as the W-M field. (The following parameters were employed: $R_1 = 10\ R_E$, $R_2 = 40\ R_E$, $r_b = 10\ R_E$, $B_{cs} = 40\ \gamma$, where $R_E = 1$ earth radius.) Integration of the vector field from the position of the satellite determines where the field-line intersects the magnetic equator. R_0, the geocentric distance in earth radii of this intersection, would be equivalent in a simple dipole

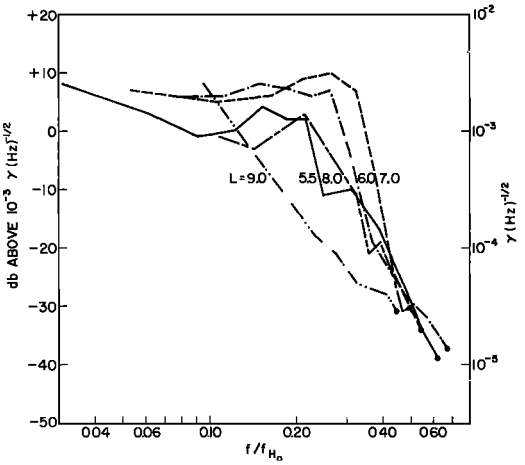

Fig. 4. Amplitude spectra normalized by f_{H0} (Williams-Mead model) for the pass shown in Figure 3. Dots at right designate point at which intensity reaches background level. Note typically rapid decrease of emission intensity with increasing frequency in vicinity of $f/f_{H0} = 0.3$.

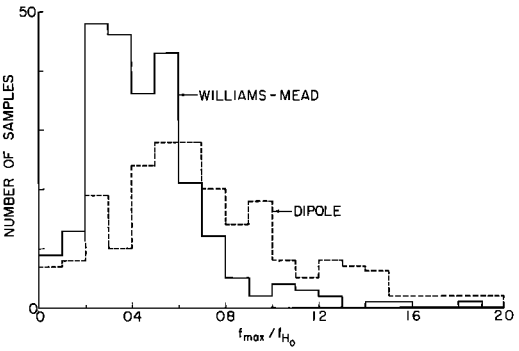

Fig. 5. Distribution of upper-cutoff frequency (f_{max}) normalized by minimum gyrofrequency (f_{H0}) for dipole and Williams-Mead models. Values greater than 2.0 are not shown; these account for 13% of the total for the dipole model and 3% for the W-M model. Values of f_{max} between 0.2 and 0.6 f_{H0} are most common. Reduced spread of data with Williams-Mead model is indicative of generation near equatorial plane.

field to L value. The local mean time is also measured with respect to this intersection. The minimum gyrofrequency measured along the distorted fieldline between the satellite and the equator may differ by a factor of 2 or more from that indicated by a single dipole field.

Measurement of the upper cutoff. The upper-cutoff frequency has been scaled from all the amplitude spectrum data by first subdividing the data into spatial sectors defined by $\Delta L = 1$ earth radius and ΔLMT = 2 hours. The sectors are centered on integer values of L and odd integer values of LMT. The inner boundary was limited by the amount of available data to $L = 2.5$ and the outer boundary to the closed fieldline region given by the W-M field model as shown in Figure 7 (to be discussed later). For each pass through a sector, represented by 10 to 450 frames of data depending upon the bit rate, the highest value of the upper-cutoff frequency was recorded along with its corresponding L value. Thus each pass through a sector generates one data point. Data samples were rejected if they included less than 0.5 R_E in L value. In this manner 274 data points were recorded, each representing 10 to 450 observations and spanning the range from 0.3 to 50 kHz. These data appear in reduced form in Figure 6, to be discussed later.

The upper-cutoff frequencies of whistler-mode emissions generally show different distributions inside and outside the plasmapause. Eighteen data points likely to represent observations inside the plasmapause were selected on the basis that the maximum Kp over the previous 24 hours was less than 3— and that L was less than 4 [*Carpenter*, 1967]. These data points are characterized by a mean value of $f_{max}/f_{H0} = 0.1$. The distribution of f_{max}/f_{H0} for the other 253 samples, which represent observations mainly outside the plasmapause, is shown by the dashed curve of Figure 5 for a simple dipole field model. The resulting distribution has a broad maximum near $f_{max}/f_{H0} = 0.6$.

Use of the W-M model of the earth's field narrows and lowers the distribution of upper cutoff frequencies, as shown by the solid curve of Figure 5. Thus the number of points for which $f_{max}/f_{H0} > 2.0$ is reduced from 34 to 7. With this model the upper-cutoff frequencies of most emissions fall in the relatively narrow range of 0.2 to 0.6 f_{H0}. The closeness of the relationship between the emission spectrum and conditions at the magnetic equator is thus enhanced when the more accurate W-M field is employed.

The upper-cutoff measurements indicate that the cutoff is more closely related to the gyrofrequency at the equator than the gyrofrequency at the satellite. This comparison is illustrated in Figure 6, which shows the normalized upper-cutoff frequency f_{max}/f_H versus f_{H0}/f_H. The latter quantity is a function of distance along a fieldline; in a purely dipole field it would be a simple function of the magnetic latitude as shown at the top of the figure.

If the upper-cutoff frequency were under local rather than equatorial control, the height of the data points above the base of the graph would not vary with position along the horizontal axis. Instead the data points tend to fall along a line of positive slope passing through the origin, indicating that the upper-cutoff frequency is proportional to f_{H0}. The median computed for 10 equally spaced intervals along the x axis and shown by the dashed line lies near $f_{max} \approx 0.45\ f_{H0}$.

It is useful to consider those few points for which f_{max} is near or above f_{H0}. Most have been categorized as one of the following: (1) emissions occurring at a discrete frequency close to,

and moving with, the local gyrofrequency (these points are shown boxed); (2) emissions associated with the plasmapause; (3) emissions recorded on the dayside at great distances from the earth where the estimates of the magnetic field may be in error; (4) hiss-like emissions observed on the nightside near or outside the plasmapause that often display a lower cutoff above 1 kHz. The latter may represent observations of auroral hiss.

The points in Figure 6 for which $f_{max} < 0.2\ f_{H0}$ probably represent observations within the plasmasphere. For instance, the points shown circled nearly all occur at low ratios of f_{max}/f_{H0}, and these points were selected as discussed previously to insure that they occurred inside the plasmasphere. Furthermore, values of $f_{max} < 0.2\ f_{H0}$ are rare well outside the usual position of the plasmasphere.

We conclude that the cutoff frequency observed outside the plasmasphere tends to be (1) independent of position along a given fieldline and (2) proportional to f_{H0}. The cutoff frequencies outside the plasmasphere generally lie between 0.2 and 0.6 f_{H0}, whereas inside they lie below 0.2 f_{H0}.

Interpretation of the upper cutoff. The fact that the cutoff frequency is proportional to f_{H0} does not by itself prove that generation occurs at the equator. Generation at any fixed latitude

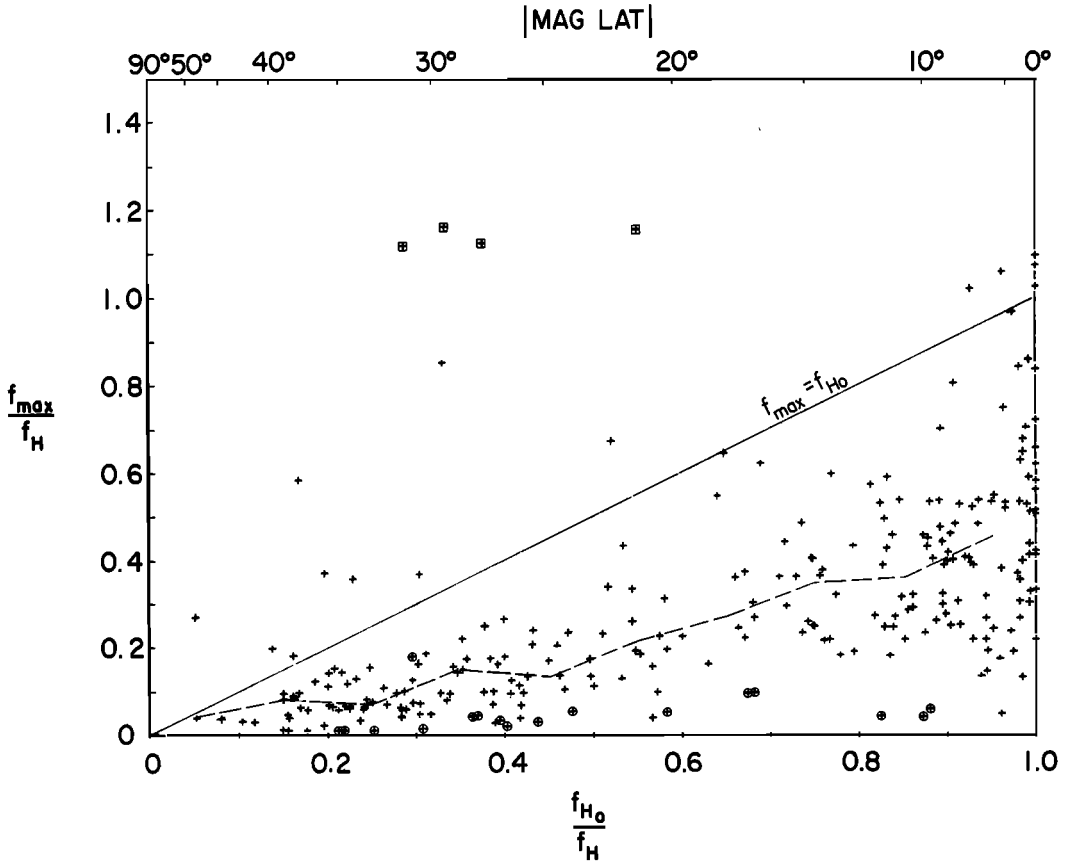

Fig. 6. Scatterplot of the upper-cutoff frequency f_{max} normalized by f_H and plotted versus f_{H0}/f_H, a function of distance along the fieldline. The Williams-Mead model was used to compute f_H and f_{H0}. Equivalent magnetic latitudes for given f_{H0}/f_H in a dipole field are shown at top of figure. The dashed line representing the median of the data lies near $f_{max} = f_{H0}/2$, indicating upper-cutoff frequency is proportional to f_{H0} rather than f_H. Circled points represent data most likely obtained within plasmasphere. Boxed points represent narrowband disturbances associated with f_H.

ϕ is possible since $f_H(\phi, L)/f_{Ho}(L)$ is constant for all L. However, generation over a wide range of latitudes is not compatible with the observed invariance of the cutoff along a fieldline.

The latitude at which generation does occur may be inferred from the differences between the shapes of the distributions of f_{max}/f_{Ho} shown in Figure 5 for two different models of the earth's magnetic field. The W-M field produces a narrower distribution than does the dipole field. (A measure of the relative breadth of a distribution, the variance divided by the square of the mean, is nearly twice as great for the dipole field distribution.) This implies that the correlation of the cutoff frequency is significantly better with f_{Ho} based on the W-M field than with f_{Ho} based on a dipole field. Significant differences in the fields based on the two models are confined to low magnetic latitudes: near the noon meridian at $R_0 = 9$ values of f_{Ho} predicted by the two models differ by a factor of 5.5, whereas values of f_H at 40° latitude differ by only 12%. Hence the improved correlation of the cutoff frequency with f_{Ho} based on the W-M field implies that the emissions are governed by conditions near the magnetic equator.

We conclude that emissions are generated near the magnetic equator. This conclusion is supported by the fact that away from the equator no known features make any one magnetic latitude more appropriate than any other. At the equator, however, there occurs a minimum in f_H as well as a change in the topology of the refractive index surface since there $f_{max}/f_H \sim 0.5$ [*Burtis and Helliwell*, 1969].

Burtis and Helliwell [1969] have shown that the ratio of the center frequency of banded chorus to the minimum gyrofrequency decreases significantly with magnetic latitude. This is explained by an inward deviation of a nonducted ray path from the field-aligned paths assumed here. Similarly, ray paths of waves generated at frequencies below $f_{Ho}/2$ tend to deviate outward from the magnetic field [*Thorne and Kennel*, 1967]. In the range of magnetic latitudes traversed by OGO 1 (normally <45°), both deviations are believed to be relatively small. Hence these effects do not alter the conclusions of the present paper.

Intensity measurements. The intensity of whistler-mode emissions has been measured from the OGO 1 amplitude spectra by subdividing the data into L-LMT sectors in a manner analogous to the measurement of upper-cutoff frequencies. Within each sector the maximum intensity at frequencies $f \geq 0.3$ kHz was recorded regardless of the frequency at which it occurred. The spectrum below 0.3 kHz was omitted because of the high background level as shown in Figure 1*b*. If no emissions were observed, the maximum background level (usually at 300 Hz) was recorded. The background level remained fairly constant except for easily identified interference from another experiment.

Using the 3-db bandwidth of the receivers, the levels were converted into the equivalent magnetic field in a 1-Hz bandwidth. As in the case of the upper-cutoff frequencies, each data point represents from 10 to 450 individual measurements (frames) within a sector. Each pass produces one point per sector. Of the recorded peak intensities 84% occur between 0.3 and 0.5 kHz, the largest proportion of which lie at 0.3 kHz. From this we may conclude that (1) the amplitude spectrum of whistler-mode emissions tends to decrease with increasing frequency above 0.3 kHz; and (2) the peak intensity data are a good measure of the intensity in the range 0.3 to 0.5 kHz. As discussed in the Appendix, the average intensity may be derived from these peak intensity measurements.

An analysis of the intensities for magnetic latitude variations is considerably more difficult than the corresponding analysis of the cutoff frequency given earlier. The difficulty is due to the irregularity of the intensity and the consequent problems associated with comparing data collected at different seasons of the year and at different telemetry rates. We may summarize our findings: (1) Intensity is independent of magnetic latitude in the range 15°–50°; (2) there may be a tendency toward weaker intensities in the range 0°–15° except in the region outside the plasmasphere at 06 $\leq$ LMT $<$ 14, where equatorial intensities are similar to those at higher latitudes.

Equatorial map of intensity. For the purpose of developing a map of the emission intensity in the vicinity of the equatorial plane, we assume that the intensity is independent of magnetic latitude. We also assume that the deviations of the ray from the W-M fieldlines

are negligible. Lastly, we use local rather than magnetic time, the difference between the two being small at magnetic latitudes less than 50°.

The resulting distribution of peak emission intensity near the magnetic equatorial plane is shown in Figure 7. The numbers represent the average peak intensity in db above 10^{-3} γ $Hz^{-1/2}$ within a sector. The average includes background levels in the absence of emissions and was computed after the intensities in descibels had been converted to their linear equivalent. Values that include only background levels are designated by <. (One particularly high background value of 3 db was produced by an un-

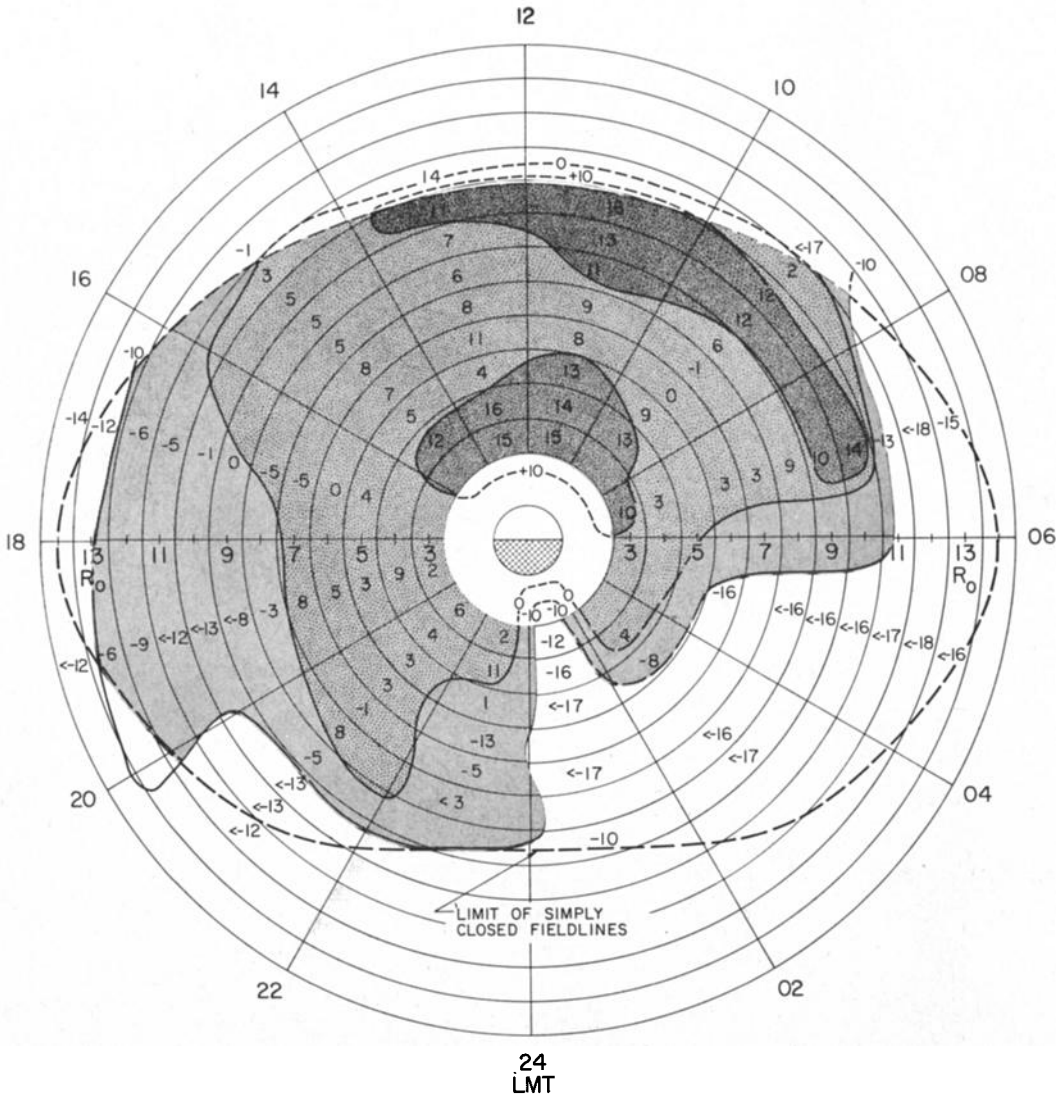

Fig. 7. Intensity of whistler-mode emissions during solar minimum as mapped along Williams-Mead fieldlines onto equatorial plane. Each number represents the average of the peak intensities in each pass through one LMT-R_0 block in db above 10^{-3} γ $(Hz)^{1/2}$. Values indicated by < contain no emissions above background level. Note two regions of intense emissions near noon meridian and centered on $R_0 = 4$ and 10. In region beyond $R_0 = 6$, little or no noise is detected in the midnight to dawn sector. Strong noise develops abruptly at dawn.

usually high level of interference from an interfering experiment.) Sectors for which no data are available appear without numbers and are drawn with the predominant shading appearing at two or more sides. The thick dashed line represents the approximate locus of the maximum R_0 for a simply closed fieldline, defined on the basis of the W-M field model as a fieldline that crosses the magnetic equator on the sun side of the tail sheet. Several values, such as the 14 at $10.5 < R_0 < 11.5$ and $12 <$ LMT < 14 represent data recorded in the shaded part of the sector although the numbers themselves fall in an unshaded region. The general consistency of the intensities in adjacent sectors implies that the given values are representative.

Smoothed contours at 10-db intervals were generated by computing an average intensity at each four-way intersection of sectors and fitting the contours upon these averages. In areas of little or no data, the estimated position of the contour is shown dashed. Crowding near the outer limit of data close to the noon meridian forced the estimated contours to fall outside their correct position, which is within the region of simply closed fieldlines.

Emission activity peaks near the 10 o'clock meridian at $R_0 \sim 4$ and $R_0 \sim 10$ with a trough of weaker activity lying between. This pattern is also observed on individual passes. Intense emissions similar to those of Figure 1 appear on the dayside inside the approximate location of the plasmapause ($R_0 = 4$); outside the plasmapause there appear discrete emissions which are similar to those of Figure 2*a*, but which tend to be of relatively low intensity below $R_0 \sim 8$. The outer region ($8 \leq R_0 \leq 11$) of intense emissions shows an abrupt onset at 06 LMT where the intensity may change in two hours from the background level to levels close to the highest intensities recorded. By contrast, the afternoon decrease in activity is much more gradual. The intensities appear to be somewhat higher with increased Kp during morning hours in accordance with the occurrence observations of *Burtis* [1969], and somewhat lower with increased Kp from late afternoon to midnight.

A broad region of space lying on the nightside between the dusk and dawn meridians and approaching as close as $R_0 = 5$ is characterized by emission intensities near the threshold level. It is in this region that the so-called highpass and broadband noises observed by the same equipment tend to occur [*Dunckel et al.*, 1969].

The variation of intensity presented here as a local-time variation could conceivably be considered as a seasonal variation since a close association exists between local time and the season of the year. However, such an interpretation is unlikely in light of emission activity on the ground, where there appear gross local-time variations in occurrence but relatively little seasonal variations for $L < 2$ [*Laaspere et al.*, 1964].

Discussion and Conclusions

Cyclotron resonance mechanisms. The upper-frequency cutoff data is, we believe, the first direct experimental evidence that VLF emissions are generated near the equatorial plane of the magnetosphere. This finding supports theories of emission generation that are based on electron cyclotron interaction in the vicinity of the minimum in the earth's magnetic field [*Brice*, 1964; *Kimura*, 1967; *Helliwell*, 1967]. From the resonance condition employed in these theories, we can estimate the energy of the resonance electrons. For the active region shown in Figure 7 at $R_0 \sim 9$, $06 <$ LMT < 14, where $f_{H0} \sim 2$ kHz and plasma frequency $\sim$15 kHz, we find for the observed frequency range of emissions (0.3 to $\sim$1 kHz) that the energy of cyclotron resonant electrons with low pitch angles ranges from approximately 10 kev down to 1 kev. In the same region *Vasyliunas* [1968] has found strong fluxes of electrons within this energy range, giving further support to theories based on electron cyclotron resonance.

Comparison with other VLF experiments. In an investigation of the occurrence of ELF emissions in the magnetosphere on OGO 3 [*Russell et al.*, 1969], emissions are categorized as either bursts or steady noise. Bursts are defined as signals that rise and fall in less than two minutes and reach a level >2 volts at either 30, 100, 300, or 800 Hz. Steady noise is defined as noise that persists (or changes intensity slowly) over two minutes at either 100, 300, or 800 Hz. The long decay time of the detector (30 sec) is likely to cause chorus with closely packed elements or with a hiss back-

ground to be identified as steady noise but no high-resolution spectra are available to check this possibility.

For burst noise the same conclusions are drawn regarding equatorial control as from the present experiment. However, from the increased occurrence of steady noise on the dayside in the region $6 \leq L < 10$ at magnetic latitudes greater than 30°, Russell et al. conclude that steady noise is generated at a latitude of about 45°. This conclusion differs from ours based on the upper-cutoff data discussed here.

A peak in 'steady' noise intensity at 45° latitude might also be explained in ways other than in terms of local generation. If we assume that generation occurs at the equator, as suggested by our cutoff data, the following interpretations of the 45° peak seem possible: (1) Emissions generated at the equator are amplified further down the fieldline as proposed by *Liemohn* [1967]; (2) an increase in the relative amount of nonducted propagation from higher magnetic latitudes could concentrate the energy at 45°; (3) the scattering of ducted emissions near the base of the fieldline could cause a maximum in occurrence at high latitudes.

Certain features in the intensity map of Figure 7 also appear in the occurrence maps reported by Russell et al. The region of intense emissions near LMT $\sim$ 10 and $R_0 \sim 4$, for instance, is very similar to the active region of steady noise shown in Russell's Figure 4. The major difference is an onset time $\sim$06 hours in Figure 7 compared with $\sim$04 hours for the Russell data. This discrepancy may result from the higher level of magnetic activity that characterizes the Russell data sample. A similar shift to earlier onset times for disturbed magnetic conditions has been seen in emissions recorded at high-latitude ground stations [*Laaspere et al.*, 1964].

The occurrence of VLF emissions has been measured at low altitudes by Injun 3 [*Taylor and Gurnett*, 1968]. Many of the features discussed in connection with Figure 7 appear in their map of invariant latitude versus local mean time, including the sudden onset near 06 hours, the active day region from 06 to 14 hours, and the quiet nightside. However, little activity is shown at invariant latitudes greater than 75° or $R_0 \sim 9$ near the noon meridian. One explanation is the diminished sensitivity of the Injun 3 receiver at the low frequencies where the emissions at high R_0 are most likely to occur. Another is that the burst-like nature of the emissions at high R_0 will tend to reduce the occurrence index even though the intensity may be high.

Intensities from the two receivers have been compared at $L = 5$, where a peak in intensity appeared in Injun 3 data in the sector 06 < LMT < 13 [*Gurnett and O'Brien*, 1964]. Compensation for the frequency response of the Injun 3 receiver and for the estimated refractive index at both satellites shows that both OGO 1 and Injun 3 observe approximately the same power density at this L value. Because of the strong convergence of magnetic fieldlines, we might expect the power density to increase markedly with latitude (by a factor of roughly 100 from the equator to 1000 km altitude at $L = 5$). The fact that it does not may indicate the presence of attenuation factors.

Modes of propagation. It is possible for emission energy to be confined to field-aligned irregularities (ducts) or to be loosely guided along the magnetic field in the 'nonducted' mode. Evidence for the latter hypothesis is the continuity of the emissions and the absence of localized spatial variations in the spectrum, as shown in Figure 3. Evidence for ducting is the occurrence of localized variations in intensity and spectrum. Enhancements of emission intensity of as much as 13 db have been observed over distances $\Delta R_0 \sim 0.06$, the same equatorial duct width estimated by *Smith and Angerami* [1968] from whistler studies. We conclude that propagation of emissions to the satellite probably occurs in both ducted and nonducted modes, just as in the case of whistlers.

Wideband intensity. An average wideband emission intensity may be obtained by integrating the magnetic spectral density over the spectrum and over all local times. Based on the previous conclusions, estimates of the measured wideband intensity were made from Figure 7 as discussed in the Appendix. The estimated accuracy of the resulting wideband noise intensities is $\pm$10 db and their range is given in Table 2 versus R_0. Also shown are the field intensities required by *Kennel and Petschek* [1966] to explain the maximum flux of trapped electrons.

At each radial distance the required intensity falls within the range estimated from the data,

TABLE 2. Integrated Emission Intensities

R_0	4	5	6	7
Integrated intensity, milligammas	6 to 60	1.7 to 17	1.5 to 15	1.4 to 14
Kennel and Petschek required intensity, milligammas	20	10	8	6

thus giving support to the Kennel-Petschek theory. However, the range of uncertainty of both the theoretical and experimental estimates is too large to provide a convincing test. Simultaneous particle and wave intensity data should be used in further comparisons of this type.

Appendix

Derivation of the wideband magnetic intensity. (1) From Figure 7 the intensities at a given R_0 were converted to linear values and averaged over all local times, empty boxes being filled with estimates based on the surrounding values. (2) This average over local time of peak values was then reduced to an average intensity by subtracting 12 db at $R_0 = 4$ (assumed to be inside the knee) and 17 db at $R_0 \geq 5$ (assumed to be outside the knee) as discussed later. (3) The contribution to the wideband intensity for frequencies above 0.3 kHz was included by assuming that the emission intensity was measured at 0.3 kHz and that the intensity in gammas was proportional to (frequency)$^{-2}$, the typical spectral shape as discussed under 'Typical Emissions.' (4) The contribution below 300 Hz was included by assuming a constant intensity between 100 and 300 Hz, an assumption in accord with preliminary data from the OGO 3 search-coil magnetometer [*Russell et al.*, 1968], which indicates that signals are strongest in the range 100–300 Hz. (5) The resulting intensity values were increased by 3 db to account for the difference between noise bandwidth and the assumed 3-db bandwidth of the sweeping receivers. Note that assumptions 3 and 4 together are equivalent to assuming a total effective bandwidth of 300 Hz, which is also a not unreasonable estimate of the bandwidth of a discrete emission. This effective bandwidth is not particularly sensitive to the choice of spectral shape. Assuming the intensity to be proportional to f^{-1} rather than f^{-2} results in a change in wideband intensity of only 2 db.

Peak versus mean intensity. The relationship between the peak and mean intensity may be obtained from the distribution of the intensity about the mean and the spatial and temporal variations of the mean. Data were obtained during a period when the mean was approximately constant. The resulting number of samples versus intensity decreases so rapidly near the peak intensity that the difference of 8 db between peak and mean values is essentially independent of the number of samples.

Spatial and temporal variations were estimated from a satellite pass covering $2 \leq R_0 \leq 10$ on the dayside. The maxima were found to lie ~4 and ~9 db above the mean inside and outside the plasmasphere, respectively. Consequently the difference between mean and peak values is ~12 db inside and ~17 db outside the plasmasphere.

Acknowledgments. The authors have benefited from many discussions with their colleagues. J. Angerami made essential contributions to the programming of the vector magnetic field integrations. G. Mead supplied the subprogram that computed the vector magnetic field.

This research was supported by the National Aeronautics and Space Administration under contracts NAS 5-2131 and NGR 05-020-288, and under grant NSG 174-SC/05-020-008. Computer time for this research was partially funded by the Office of Computer Sciences in the Mathematical Division of the National Science Foundation under grant NSF GP-948.

References

Barrington, R. E., J. S. Belrose, and D. A. Keeley, Very low frequency noisebands observed by the Alouette 1 satellite, *J. Geophys. Res., 68*, 6539, 1963.

Barrington, R. E., Some satellite observations of VLF resonances, *Proc. NATO Advanced Study Inst. on Plasma Waves in Space and in the Laboratory, Røros, Norway, April 17–26, 1968*, North-Holland Publishing Co., in press, 1969.

Brice, N., Qualitative explanation of the diurnal variation of chorus, *J. Geophys. Res., 69*, 4701, 1964.

Burtis, W. J., VLF chorus observed on OGO satellites, SEL-69-019, Radioscience Labora-

tory, Stanford Electronics Laboratories, Stanford University, Stanford, Calif., August, 1969.

Burtis, W. J., and R. A. Helliwell, Banded chorus —a new type of VLF radiation observed in the magnetosphere by OGO 1 and OGO 3, *J. Geophys. Res., 74,* 3002, 1969.

Carpenter, D. L., Relations between the dawn minimum in the equatorial radius of the plasmapause and *Dst, Kp,* and local *K* at Byrd Station, *J. Geophys. Res., 72,* 2969, 1967.

Ficklin, B. P., W. E. Blair, J. H. Wensley, M. E. Mills, N. D. Schlosser, and W. H. Zwisler, OGO 1 VLF experiment A-17 digital data processing system, *Final Rept.,* Stanford Research Institute, Menlo Park, Calif., April 1967.

Dunckel, N., B. Ficklin, L. Rorden, and R. A. Helliwell, Low-frequency noise observed in the distant magnetosphere with OGO 1, in preparation, 1969.

Gurnett, D. A., and B. J. O'Brien, High-latitude geophysical studies with satellite Injun 3, 5, Very-low-frequency electromagnetic radiation, *J. Geophys. Res., 69,* 65, 1964.

Helliwell, R. A., *Whistlers and Related Ionospheric Phenomena,* Stanford University Press, Stanford Calif., 1965.

Helliwell, R. A., A theory of discrete VLF emissions from the magnetosphere, *J. Geophys. Res., 72,* 4773, 1967.

Holzer, R. E., M. G. McLeod, and E. J. Smith, Preliminary results from the OGO 1 search coil magnetometer: Boundary positions and magnetic noise spectra, *J. Geophys. Res., 71,* 1481, 1966.

IG Bulletin, OGO 1, First U. S. Orbiting Geophysical Observatory, *Trans. Am. Geophys. Union, 46,* 326, 1965.

Jørgensen, T. S., Interpretation of auroral hiss measured on OGO 2 and at Byrd Station in terms of incoherent Cerenkov radiation, *J. Geophys. Res., 73,* 1055, 1968.

Kennel, C. F., and H. E. Petschek, Limit on stably trapped particle fluxes, *J. Geophys. Res., 71,* 1, 1966.

Kimura, I., On observations and theories of the VLF emissions, *Planetary Space Sci., 15,* 1427, 1967.

Laaspere, T., M. G. Morgan, and W. C. Johnson, Chorus, hiss, and other audio-frequency emissions at stations of the whistler-east network, *Proc. IEEE, 52,* 1331, 1964.

Liemohn, H. B., Cyclotron resonance amplification of VLF and ULF whistlers, *J. Geophys. Res., 72,* 39, 1967.

Martin, L. H., R. A. Helliwell, and K. R. Marks, Association between aurorae and very low frequency hiss observed at Byrd Station, Antarctica, *Nature, 187,* 751, 1960.

Rorden, L. H., L. E. Orsak, B. P. Ficklin, and R. H. Stehle, Instruments for the Stanford University/Stanford Research Institute VLF experiment (4917) on the EOGO satellite, *Instrument Rept.,* Stanford Research Institute, Menlo Park, Calif., 1966.

Russell, C. T., R. E. Holzer, and E. J. Smith, Magnetic fluctuations between 30 and 1000 Hz within the magnetosphere, *Trans. Am. Geophys. Union, 49,* 259, 1968.

Russell, C. T., R. E. Holzer, and E. J. Smith, OGO 3 observations of ELF noise in the magnetosphere, 1, Spatial extent and frequency of occurrence, *J. Geophys. Res., 74,* 755, 1969.

Scarf, F. L., R. W. Fredricks, and G. M. Crook, Detection of electromagnetic and electrostatic waves on OV3-3, *J. Geophys. Res., 73,* 1723, 1968.

Smith, R. L., and J. J. Angerami, Magnetospheric properties deduced from OGO 1 observations of ducted and nonducted whistlers, *J. Geophys. Res., 73,* 1, 1968.

Taylor, H. A., Jr., H. C. Brinton, and C. R. Smith, Positive ion composition in the magnetoionosphere obtained from the OGO-A satellite, *J. Geophys. Res., 70,* 5769, 1965.

Taylor, W. L., and D. A. Gurnett, The morphology of VLF emissions observed with the Injun 3 satellite, *J. Geophys. Res., 73,* 5615, 1968.

Thorne, R. M., and C. F. Kennel, Quasi-trapped VLF propagation in the outer magnetosphere, *J. Geophys. Res., 72,* 857, 1967.

Vasyliunas, V. M., Low-energy electrons on the dayside of the magnetosphere, *J. Geophys. Res., 73,* 7519, 1968.

Williams, D. J., and G. D. Mead, Nightside magnetosphere configuration as obtained from trapped electrons at 1100 kilometers, *J. Geophys. Res., 70,* 3017, 1965.

(Received May 2, 1969;
revised July 24, 1969.)